# Modeling secondary organic aerosol formation from volatile chemical products

Elyse A. Pennington[1,2], Karl M. Seltzer[1], Benjamin N. Murphy[3], Momei Qin[1,4], John H. Seinfeld[2],

5   Havala O.T. Pye[3]

[1]Oak Ridge Institute for Science and Education Fellow in the Office of Research and Development, US Environmental Protection Agency, Research Triangle Park, NC 27711

[2]Department of Chemical Engineering, California Institute of Technology, Pasadena, CA 91125

[3]Office of Research and Development, US Environmental Protection Agency, Research Triangle Park, NC 27711

10  [4]Jiangsu Key Laboratory of Atmospheric Environment Monitoring and Pollution Control, Collaborative Innovation Center of Atmospheric Environment and Equipment Technology, School of Environmental Science and Engineering, Nanjing University of Information Science & Technology, Nanjing, China

*Correspondence to*: Havala O.T. Pye (Pye.Havala@epa.gov)

**Abstract.** Volatile chemical products (VCPs) are commonly-used consumer and industrial items that are an important source
15 of anthropogenic emissions. Organic compounds from VCPs evaporate on atmospherically relevant time scales and include
many species that are secondary organic aerosol (SOA) precursors. However, the chemistry leading to SOA, particularly that
of intermediate volatility organic compounds (IVOCs), has not been fully represented in regional-scale models such as the
Community Multiscale Air Quality (CMAQ) model, which tend to underpredict SOA concentrations in urban areas. Here we
develop a model to represent SOA formation from VCP emissions. The model incorporates a new VCP emissions inventory
20 and employs three new classes of emissions: siloxanes, oxygenated IVOCs, and nonoxygenated IVOCs. VCPs are estimated
to produce 1.67 μg m$^{-3}$ of noontime SOA, doubling the current model predictions and reducing the SOA mass concentration
bias from -75% to -58% when compared to observations in Los Angeles in 2010. While oxygenated and nonoxygenated
intermediate volatility VCP species are emitted in similar quantities, SOA formation is dominated by the nonoxygenated
IVOCs. Formaldehyde and SOA show similar relationships to temperature and bias signatures indicating common sources
25 and/or chemistry. This work suggests that VCPs contribute up to half of anthropogenic SOA in Los Angeles and models
must better represent SOA precursors from VCPs to predict the urban enhancement of SOA.

## 1 Introduction

30

Organic aerosol (OA) is a major component of fine particulate matter (PM$_{2.5}$) in urban areas throughout the world (Zhang et
al., 2007). PM$_{2.5}$ influences human health (Lim et al., 2012), climate (Intergovernmental Panel on Climate Change, 2014),
and visibility (Hyslop, 2009), so understanding OA composition is an important step in mitigating the adverse effects of
PM$_{2.5}$. Secondary organic aerosol (SOA) is often the dominant component of OA (Jimenez et al., 2009) and is formed when
35 gas-phase volatile organic compounds (VOCs) react with atmospheric oxidants to form products that condense into the
aerosol phase, where they can undergo further reaction. SOA is formed via thousands of atmospheric reactions (Goldstein &
Galbally, 2007), so understanding its sources remains a challenge.

Volatile chemical products (VCPs) are an important source of organic emissions that lead to SOA formation (McDonald et
40 al., 2018; Qin et al., 2021). As vehicle exhaust becomes cleaner and mobile source emissions decline, the relative importance
of VCP emissions increases (Khare & Gentner, 2018). Previous work suggests that during the 2010 California Nexus of Air
Quality and Climate Change (CalNex) campaign in Southern California (Ryerson et al., 2013), VCPs contributed
approximately 1.1 μg m$^{-3}$, or 41%, of observed SOA above background levels in the Los Angeles Basin (Qin et al., 2021).

45 Modeling the formation of SOA in three-dimensional (3D) chemical transport models (CTMs) is challenging due to the
complexity of VOC chemistry and computational constraints of regional-scale modeling. Models have tended to
underpredict SOA mass in urban locations for a variety of reasons. For one, the SOA formation potential of intermediate

volatility organic compounds (IVOCs) and semivolatile organic compounds (SVOCs) – or S/IVOCs – is not well constrained. Observations made during the CalNex campaign demonstrate that S/IVOCs are important sources of SOA, making up only 10% of total gas-phase organic compound concentrations (Zhao et al., 2014) while contributing up to 80% of above-background SOA mass (Hayes et al., 2015). Although it is often impossible to identify all individual species contributing to ambient S/IVOCs, these compounds may be classified based on their properties (e.g. volatility). Volatility basis set (VBS) models (Donahue et al., 2011) are often used to represent S/IVOC chemistry and partitioning, and have improved model estimates of SOA (Woody et al., 2016; Hayes et al., 2015; Robinson et al., 2007). Murphy et al. (2017) integrated a VBS model into the Community Multiscale Air Quality (CMAQ) model version 5.2 to represent the multigenerational aging of semivolatile primary organic aerosol (POA) leading to the production of SOA. Other studies have parameterized VBS models to represent S/IVOCs from mobile emissions (Lu et al., 2020; Jathar et al., 2017), but none have parameterized SOA formation from VCP S/IVOCs emissions. Additionally, the emissions of S/IVOCs are not well constrained and are often not included in detailed emissions inventories (Zhao et al., 2015). However even when S/IVOCs are included in emissions inventories, they are often assigned to nonreactive or nonvolatile model surrogates that do not participate in model chemistry (T. Shah et al., 2020). Improving the representation of SOA chemistry in CMAQ will allow for more accurate exposure estimates in health studies and source apportionment for air quality management decisions.

Another source of error in CTMs is the lack of representation of oxygenated SOA precursors. Historically, mechanism development has focused on the oxidation chemistry of species emitted primarily from vehicles (e.g. BTEX: benzene, toluene, ethylbenzene, and xylene) or biogenic sources (e.g. isoprene, monoterpenes). While VCPs do emit some of these species, they also emit many oxygenated compounds (Seltzer et al., 2021; McDonald et al., 2018). The implications of a few important oxygenated precursors on air quality have recently been quantified (e.g. Janechek et al., 2017; Charan et al., 2020; L. Li & Cocker, 2018; W. Li et al., 2018), but many oxygenated precursors have not been studied in a laboratory setting. For the few oxygenated VCPs that have been studied in laboratory chambers, SOA yields were reported under unrealistic atmospheric conditions, e.g. high OH and aerosol seed concentrations. So, the SOA yields of these compounds have primarily been estimated using models such as the Statistical Oxidation Model (SOM; Cappa & Wilson, 2012) or VBS (McDonald et al., 2018; R. U. Shah et al., 2020). These oxygenated species are not included as SOA precursors in most models, and their chemistry is needed to improve predictions of SOA mass.

In this work, we introduce a chemical mechanism to represent SOA formation from VCPs. Specifically, the potential of both oxygenated and nonoxygenated IVOCs to form SOA is developed and evaluated. We utilize a new VCP emissions inventory known as VCPy (Seltzer et al., 2021) to represent organic emissions from VCPs and to parameterize model species behavior in the chemical mechanism. The chemistry and emissions inventory are implemented in the Community Multiscale Air Quality (CMAQ) model version 5.3.2 to simulate air quality during the CalNex campaign in California in 2010. The model

predictions are compared to measurements made in Pasadena during CalNex and the speciation of predicted SOA is examined.

## 2 Methods

85

### 2.1 VCPy emissions inventory implementation

VCPy is a modeling framework that estimates reactive organic carbon emissions from VCPs (Seltzer et al., 2021). Within this framework, the complete VCP sector is disaggregated into several product use categories (PUCs; e.g. cleaning products,

90 personal care products, adhesives and sealants, paints and coatings). U.S. nationwide usage of each PUC is estimated, and survey data are then used to quantify the mass fraction of organic, inorganic, and water proportions, as well as speciate the organic fraction. Physiochemical properties of each organic component are used to estimate the characteristic evaporation timescale, which is then compared to an assigned use timescale to determine whether a compound is retained or evaporated from each PUC. In the initial implementation of VCPy (version 1.0), which is representative of 2016 conditions, the

95 predicted nationwide and Los Angeles County VCP emission rates were 9.5 kg person$^{-1}$ year$^{-1}$ and 8.2 kg person$^{-1}$ year$^{-1}$, respectively. These emission rates are consistent with the low end of values seen in a previous study that used a top-down approach to estimate VCP emissions (Qin et al., 2021). In our work, product use is based on data from 2010 with composition specified using data from the early 2000s to overlap with the CalNex campaign.

100 Since the speciation of organic emissions from VCPy is explicit, the underlying chemical and physical properties of emissions are output from the framework. These properties, many of which are relevant to atmospheric oxidation and subsequent SOA formation, include the oxidation rate with the hydroxyl radical ($k_{OH}$), molecular weight (MW), volatility (C*), and oxygen-to-carbon ratio (O:C). SOA mass yields, which are defined as the mass of SOA formed per mass of ROC precursor reacted, were assigned based on compound-specific structure and volatility (Seltzer et al., 2021).

105

A key step in implementing this inventory into CMAQ is ensuring that all compounds predicted to be emitted by VCPy are mapped to either an existing or a new model surrogate. Emissions of low-volatility organic vapors (C* < $10^{6.5}$ µg m$^{-3}$) from all sources are prime SOA precursors but traditionally discarded from the gas-phase chemical mechanism used in many CTMs (e.g. represented as nonvolatile (NVOL), nonreactive (NROG), or unspecified IVOC species that are not used in the

110 chemical mechanism of CMAQ; Carter, 2010). As a result, these species do not participate in atmospheric chemistry and thus do not impact radical concentrations or SOA mass. In addition, oxygenated compounds are not currently included as SOA precursors in many mechanisms because of the historic focus on SOA formation from nonoxygenated vehicle exhaust and traditional VOCs like single-ring aromatics and biogenic hydrocarbons. The work of Qin et al. (2021) specifically identifies this loss of emitted reactive carbon mass as a reason for underestimated SOA from the personal care sector in the

115 CMAQ model. To account for the SOA potential of this previously neglected organic mass, all compounds currently mapped
to NROG, NVOL, and IVOC are reviewed, with most of this mass routed to one of three newly added categories of model
surrogates: siloxanes (SILOX), oxygenated IVOCs (SOAOXY), and nonoxygenated IVOCs (IVOCP3, IVOCP4, IVOCP5,
IVOCP6, IVOCP5ARO, and IVOCP6ARO). The updated mechanism (with SOA pathways described in Section 2.2) with
the newly implemented speciation mapping is henceforth described as SAPRC07TIC_AE7I_VCP and the complete list of
120 assignment rules is provided in the SI Methods. In summary:

(1) All silicon-containing species (including siloxanes and silanes) are assigned to SILOX.

(2) Species assigned to low-volatility, inactive species (i.e. NVOL, NROG, or IVOC) whose ozone and SOA formation
are not otherwise captured in existing gas-phase surrogates are assigned to the new IVOC surrogates (SOAOXY,
125 IVOCP3/4/5/6/5ARO/6ARO) or an existing long alkane surrogate (SOAALK) according to their structure, O:C,
$C^*$, and SOA yield.

(3) All species assigned to SOAOXY, IVOCP3/4/5/6/5ARO/6ARO, and SOAALK are also mapped to existing alkane
surrogates based on $k_{OH}$ to participate in ozone chemistry. Siloxanes are not mapped to alkane surrogates because of
their low $k_{OH}$. Since these alkane species do not participate in the SOA module and the VCP surrogates do not affect
130 ozone chemistry, this double-mapping does not double-count chemistry due to the lack of overlap between these
parts of the gas- and aerosol-phase mechanisms.

(4) Some compounds were manually reassigned depending on their SOA yield.

(5) All other compounds retained their assignments to existing model surrogates.

135 County-level VCPy emissions (Seltzer et al., 2021) were gridded at 4-km scale to fit the CalNex domain (Baker et al., 2015)
using a variety of spatial surrogates. The spatial surrogates used depend on the category of VCP emissions being described:
agricultural land is used as a proxy for all agricultural pesticide emissions, the density of oil and gas wells for the oil and gas
solvent emissions, and population for all remaining VCP sources. While some categories of VCP emissions could feature
more refined spatial surrogate proxies, the uncertainty associated with spatial allocation of sources may be lower than
140 uncertainty in individual source strength. More specifically, if an entire VCP category could be matched to a single
surrogate, allocation methods would still assume there is no variation in the strength of individuals within the population of
that surrogate (Y. Li et al., 2021).

All VCP emissions feature a sinusoidal diurnal profile with a peak at noon, with no application of day-of-week or seasonal
145 profiles. Since the simulation period used in this study is a single month, no seasonal changes would be observable over this
time frame and previous work suggests little seasonal variability in VCP emissions (Gkatzelis et al., 2021). Other emission
sectors (e.g. mobile sources, agriculture) are adjusted for seasonal impacts based on meteorological conditions and known

activity data. The seasonal effects applied to other sectors of emissions, e.g. mobile source emissions, are a function of the meteorological conditions.

150

## 2.2 Parameterizing SOA formation from VCPs

To better represent the atmospheric chemistry of VCPs, SOA formation is added for the three new categories of emissions (siloxanes, oxygenated IVOCs, and nonoxygenated IVOCs) in the SAPRC07TIC_AE7I_VCP chemical mechanism within
155 CMAQ (Table 1).

Cyclic volatile methylsiloxanes (cVMS), or siloxanes for short, are present in many personal care products, adhesives, and sealants. Collectively, siloxanes represent a large fraction of VCP emissions (Seltzer et al., 2021). Decamethylcyclopentasiloxane ($D_5$-siloxane) is the most prevalent siloxane in urban atmospheres (D.-G. Wang et al., 2013)
160 and laboratory studies have found $D_5$-siloxane SOA yields ranging from 0% (Charan et al., 2021) to 50% (Janechek et al., 2019). The explicit oxidation mechanism is unknown and the SOA yields of other siloxanes are not well understood (Coggon et al., 2018). Here, siloxanes are treated separately from other oxygenated VCP species due to their anomalously low OH oxidation rate (Table 1). The mechanism of SOA formation used here utilizes an existing two-product model from Janechek et al. (2019) that was parameterized using oxidation flow reactor (OFR) experiments and photooxidation chamber
165 data from Wu & Johnston (2017). In this implementation, the OH oxidation rate constant for $D_5$-siloxane matches the rate reported in Janechek et al. (2017) and the hydroxyl radical is replenished after reaction.

Few laboratory chamber studies have investigated the oxidation processes of other oxygenated gas-phase species (e.g. Charan et al., 2020; L. Li & Cocker, 2018), so little experimental data exist about the SOA yields or oxidation products of
170 oxygenated SOA precursors. Additionally, many models that predict the products of oxidation reactions (e.g. SOM and VBS) have not been parameterized or evaluated using oxygenated precursors. Without these models and laboratory studies, little is known about the oxidation products of these precursors, which limits our ability to develop a detailed model of their SOA formation. Therefore, all non-siloxane oxygenated IVOC emissions are represented by a single surrogate (SOAOXY) that undergoes a one-step reaction with the hydroxyl radical to form a nonvolatile aerosol surrogate (AOIVOC). This simple
175 mechanism reduces the reliance on many parameters that are not well-constrained. The MW, $k_{OH}$, $C^*$, and SOA yield of this surrogate are calculated as a mass-weighted average of the oxygenated IVOC emissions from VCPs in Los Angeles County which are generally consistent with what would be calculated using nationwide information.

Nonoxygenated IVOC emissions are represented using the model described by Lu et al. (2020), which uses a VBS model
180 and multigenerational aging scheme to represent the SOA from gasoline, diesel, and aircraft sources. Six surrogates are differentiated by structure (alkane vs. aromatic) and volatility, and each is assigned a four-product yield distribution,

generating SVOCs after one oxidation step. Many of the nonoxygenated IVOC species from mobile and VCP emission sources have similar structures (i.e. long and branched alkanes and aromatics), volatilities, and SOA yields (see Fig. S1), making the Lu et al. (2020) model a good representation of oxidation and SOA formation from nonoxygenated VCP IVOCs.

185

**Table 1. Properties of the VCP surrogates added to CMAQ version 5.3.2.**

| | MW (g mol$^{-1}$) | $k_{OH}$ x 10$^{11}$ (cm$^3$ molec$^{-1}$ sec$^{-1}$) | $\alpha_i$ | C* ($\mu$g m$^{-3}$) | SOA mass yield (at 10 $\mu$g m$^{-3}$) | $H_{vap}$ (kJ mol$^{-1}$) | $\kappa_{org}$ | H (M atm$^{-1}$) | OM/OC |
|---|---|---|---|---|---|---|---|---|---|
| SILOX | 368.66[a] | 0.155[b] | - | - | - | - | - | 3.87 x 10$^{2\,f}$ | - |
| SV/ASILOX1 | 416.66[a] | - | 0.14[c] | 0.95[c] | 0.13 | 131[d] | 0.09[e] | 2.97 x 10$^{6\,f}$ | 3.49[e] |
| SV/ASILOX2 | 384.66[a] | - | 0.82[c] | 484[c] | 0.017 | 101[d] | 0.05[e] | 7.99 x 10$^{4\,f}$ | 3.22[e] |
| SOAOXY[g] | 170.95 | 2.54 | - | - | - | - | - | 2.85 x 10$^{3\,f}$ | - |
| AOIVOCJ[g] | 186.95 | - | - | - | 0.0628 | - | 0.09[e] | - | 1.73[e] |
| IVOCP3[h] | 296.6 | 2.65 | [h] | 10$^3$ | 0.43 | 52 | - | 2 x 10$^8$ | - |
| IVOCP4[h] | 254.9 | 2.25 | [h] | 10$^4$ | 0.43 | 41 | - | 2 x 10$^8$ | - |
| IVOCP5[h] | 219.4 | 1.89 | [h] | 10$^5$ | 0.35 | 30 | - | 2 x 10$^8$ | - |
| IVOCP6[h] | 184.4 | 1.55 | [h] | 10$^6$ | 0.15 | 19 | - | 2 x 10$^8$ | - |
| IVOCP5ARO[h] | 197.3 | 7.56 | [h] | 10$^5$ | 0.36 | 30 | - | 2 x 10$^8$ | - |
| IVOCP6ARO[h] | 162.3 | 3.05 | [h] | 10$^6$ | 0.25 | 19 | - | 2 x 10$^8$ | - |

[a]The gas-phase siloxane (SILOX) MW is the average of the MW of all VCPy siloxane and silane species weighted by Los Angeles County emission rates. The MW of the higher-volatility siloxane products (SVSILOX2/ASILOX2J) is approximated as the sum of the MW of SILOX and one oxygen. The MW of the lower-volatility products (SVSILOX1/ASILOX1J) has an additional two oxygens to represent its significant decrease in volatility.

[b]The siloxane $k_{OH}$ is given in Janechek et al. (2017).

[c]The stoichiometric product yields ($\alpha_i$) and C* of the siloxanes are given in Janechek et al. (2019).

[d]Enthalpy of vaporization ($H_{vap}$) values for the siloxanes are estimated according to the method in Epstein et al. (2010).

[e]All OM/OC ratios and hygroscopicity parameters ($\kappa_{org}$) are estimated using equations 5 and 12, respectively, in Pye et al. (2017).

[f]Henry's Law constants (H) at 298.15 K are estimated using the surrogate-based method in Hodzic et al. (2014).

[g]The MW, $k_{OH}$, C*, and SOA yield of SOAOXY and AOIVOCJ are calculated as a mass-weighted average of the oxygenated IVOC emissions from VCPs in Los Angeles County. Because AOIVOC is formed via a single reaction with a constant SOA yield, it is treated as nonvolatile and therefore is not assigned a C* or $H_{vap}$.

[h]All nonoxygenated IVOC surrogate properties – including four stoichiometric product yields ($\alpha_i$) for each surrogate used in the multigenerational scheme – are described in Lu et al. (2020).

## 2.3 CMAQ model implementation

### 2.3.1 CalNex model configuration

The updated chemical mechanism and VCPy-derived emissions were implemented in CMAQ version 5.3.2 (US EPA Office of Research and Development, 2020). CMAQ version 5.3 and the subsequent minor releases are documented in Appel et al. (2021). The model was used to simulate air quality during the CalNex campaign from May 15 to June 15, 2010, with an additional 14-day spin-up period. Outside the VCP updates, the model configuration matches the implementation used in Qin et al. (2021) and Lu et al. (2020). The model domain has 4-km x 4-km horizontal resolution (325 x 225 grid cells) covering California and Nevada with 36 vertical levels reaching 50 mbar. Meteorological inputs are derived from the Weather Research and Forecasting (WRF) Advanced Research WRF core Model version 3.8.1 (Skamarock et al., 2008). Gas-phase chemistry is represented using SAPRC07TIC (Pye et al., 2013; Xie et al., 2013) with the addition of the VCP chemical mechanism summarized in Table 1. Aerosol-phase chemistry is simulated using an extended version of the AERO7 mechanism, depicted in Figure 1, including all AERO7 reactions plus those of the new VCP mechanism (boxed in red) and mobile IVOCs (boxed in red in the lower left) that participate in the multigenerational aging shown in the orange boxes (Lu et al., 2020). This diagram also includes a representation of the aqueous-phase cloud chemistry and removal used in the Asymmetric Convection Model (ACM) version 2 module (Binkowski & Roselle, 2003), which has been updated to include wet deposition properties for the new aerosol surrogates (Table 1).

All non-VCP anthropogenic emissions are based on the 2011 National Emissions Inventory (NEI) version 2 (US EPA, 2015). VCP emissions in the NEI are removed and replaced with VCPy predicted emissions using the Detailed Emissions Scaling, Isolation, and Diagnostic (DESID) module (Murphy et al., 2021). Mobile $NO_x$ emissions were reduced by 25% in all simulations to better match observational data from the CalNex campaign (Qin et al., 2021). Mobile IVOC emissions and the semivolatile treatment of mobile POA were treated according to the methods described in Lu et al. (2020). The IVOCs are assigned to the appropriate IVOCP3/4/5/6/5ARO/6ARO surrogates that are also used to treat nonoxygenated IVOCs from VCPs. Wind-blown dust emissions are neglected in this study. Biogenic emissions are calculated online using the Biogenic Emission Inventory System (BEIS) version 3.6.1 (Bash et al., 2016) as are sea spray aerosol emissions.
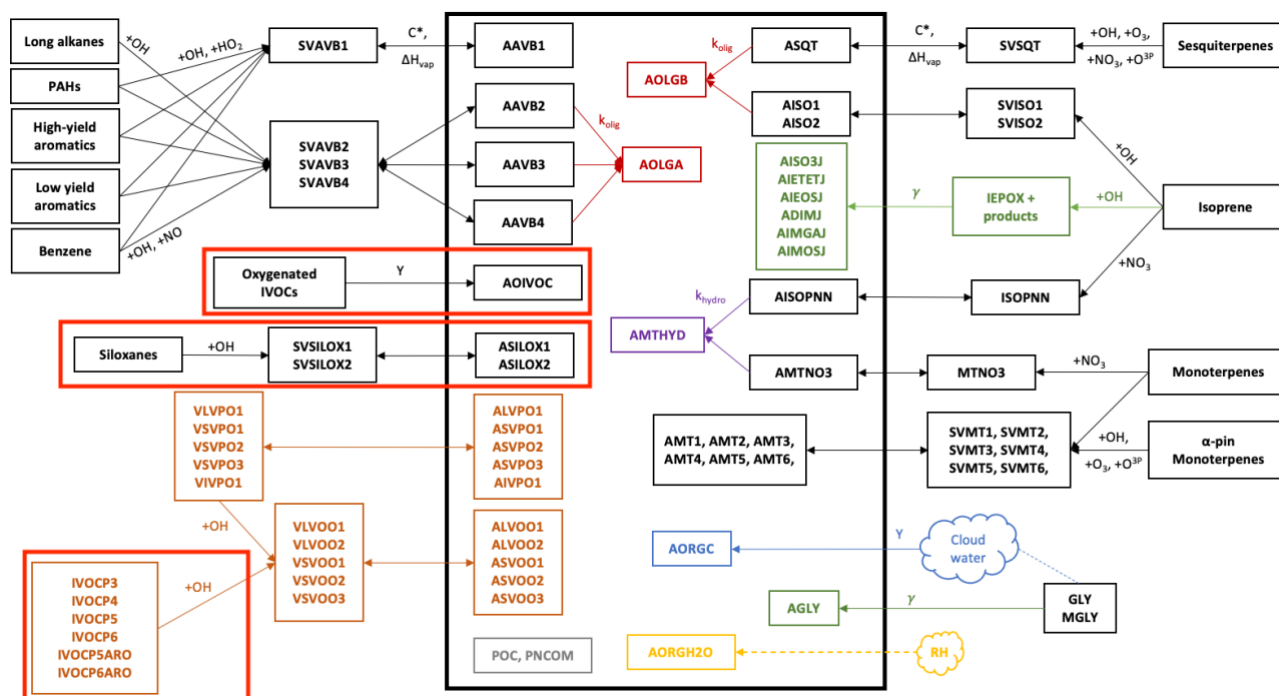
**Figure 1. Treatment of OA chemistry in the CMAQv5.3.2+VCP model. The thick black box surrounds all aerosol-phase species. All smaller black boxes depict species undergoing gas-phase oxidation from VOCs to semivolatile or nonvolatile SOA species. Orange depicts the VBS model for S/IVOCs. Red depicts particle-phase accretion reactions while purple depicts particle-phase hydrolysis reactions. Green represents heterogeneous processes. Blue shows cloud-processed aerosol and yellow shows aerosol water associated with the organic phase. Gray boxes are nonvolatile primary organic aerosol (POA) species. Double-sided arrows represent reversible processes and one-sided arrows represent irreversible processes. Dashed lines represent processes that are dependent on relative humidity. The diagram includes the AERO7 mechanism plus the three VCP-forming pathways (boxed in red). See AE7I Species Table (2016/2021) for species descriptions.**

**2.3.2 Simulation cases**

Three simulations were evaluated against the observations collected during the CalNex campaign. A "zero VCP" case removes all VCP emissions. The "CMAQv5.3.2" case is a standard CMAQ simulation with base emissions (i.e. VCP emissions from the NEI) and base chemistry (i.e. no new VCP chemistry). Finally, the "CMAQv5.3.2+VCP" case adds both the VCP chemistry described above (i.e. SAPRC07TIC_AE7I_VCP) and replaces all NEI VCP emissions with VCPy-derived VCP emissions. Comparisons between the "zero VCP" case and the "CMAQv5.3.2+VCP" case illustrate the complete impact of VCPy emissions on modeled SOA. In contrast, comparisons between the "CMAQv5.3.2" case and the "CMAQv5.3.2+VCP" case illustrate the impact of the new representation of VCP emissions and chemistry against the current status of VCPs in CMAQ. Results from the CMAQv5.3.2 case are presented primarily in the SI.

### 2.3.3 Comparison with observations

Observational data are provided by a suite of instruments deployed during the 2010 CalNex campaign in Pasadena. There
255 were two data collection sites in the CalNex campaign – Pasadena and Bakersfield – and model predictions are compared to
measurements made at the Pasadena site, which is located in the Los Angeles Basin approximately 18 km downwind of the
urban core (Ryerson et al., 2013). $PM_1$ (fine particulate matter with diameter < 1 μm) OA data were obtained with an aerosol
mass spectrometer (AMS) and have been analyzed via positive matrix factorization (PMF) to determine its composition
(Hayes et al., 2013). Formaldehyde (HCHO) data are provided in Warneke et al. (2011) and carbon monoxide (CO) data are
260 available from Santoni et al. (2014). Ozone data throughout California were obtained from the EPA AQS monitoring
network for 178 sites operating during the simulation period (US EPA, 2013). Hourly ozone concentrations were used to
calculate daily maximum 8-hour average (MDA8) ozone concentrations.

### 3 Results & Discussion

265

### 3.1 VCP emissions and implications for SOA

VCP emissions were split almost equally between species that do and do not form SOA. The SAPRC07TIC_AE7I_VCP
speciation mapping (Figure 2) indicates 56.4% ($4.8 \times 10^7$ kg $year^{-1}$) of Los Angeles County VCP emitted mass does not form
270 SOA. This mass includes small species commonly used as solvents, such as ethanol, acetone, and small alkanes. The
remaining 43.6% ($3.7 \times 10^7$ kg $year^{-1}$) of Los Angeles County emissions are assigned to model surrogates that form SOA.
3.5% of the total emissions are assigned to siloxanes, 7.8% to oxygenated IVOCs, 11.8% to nonoxygenated IVOCs, and
20.4% to traditional SOA precursors, such as long alkanes, toluene, and other aromatics. The volatility and SOA yields of
species in each category are summarized in Fig. S1.

275

Figure 2 indicates that in traditional model processing, precursors to SOA are systematically discarded from chemistry
calculations. As described in Section 2.1, there are low-volatility emissions (i.e. NROG, NVOL, and IVOC) that do not
participate in SOA or radical chemistry in traditional SAPRC07TIC_AE7I which is a key issue in representing SOA mass.
The inner ring of Figure 2 depicts the fraction of each category that was originally assigned to inactive species (NROG,
280 NVOL, and IVOC; hatched) versus other existing surrogates (solid). $2.6 \times 10^7$ kg $year^{-1}$ (30.7%) of the total VCP emissions
were originally assigned to these surrogates and did not participate in any atmospheric chemistry processes. Using the new
speciation and mechanism, $1.8 \times 10^7$ kg $year^{-1}$ (21.2% of total VCP emissions) were reassigned to surrogates that form SOA
in the model (hatched inner ring: red, blue, orange, and purple). The remaining $8.0 \times 10^6$ kg $year^{-1}$ (9.4% of total VCP
emissions; inner ring hatched green) is comprised of species with SOA yields of zero and were not reassigned to SOA-
285 forming surrogates.
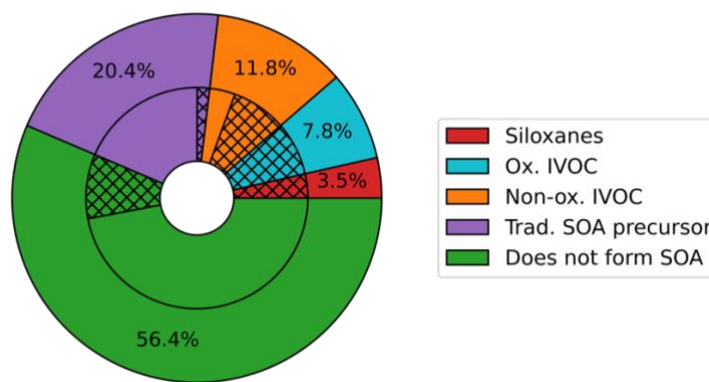
**Figure 2. Percentage of the VCP emissions assigned to each category of CMAQ surrogates using the SAPRC07TIC_AE7I_VCP speciation profiles. The total rate of VCP emissions in Los Angeles County is 8.3 x 10$^7$ kg yr$^{-1}$. The outer ring depicts the percentage of total VCPy-derived emissions assigned to each of the three new VCP categories (siloxanes in red, oxygenated IVOCs in blue, and nonoxygenated IVOCs in orange), the traditional SOA precursors described by existing model surrogates (purple), and existing surrogates that do not form SOA (green). The inner ring gives an indication of the original assignments of each of the outer ring categories. Hatching indicates emissions originally assigned to model surrogates that do not participate in model chemistry: IVOC, NVOL, and NROG. Solid colors represent other surrogate assignments.**

295 Averaged over the duration of the CalNex campaign, VCPs are predicted to be a larger source of IVOCs than mobile sources. Across mobile and VCP sources during CalNex, CMAQ predicts 6.4 μg m$^{-3}$ of the gas-phase IVOC mass is nonoxygenated and 2.6 μg m$^{-3}$ of the IVOC mass is oxygenated (Fig. S2). The observed campaign-average total IVOC concentration was 10.5 μg m$^{-3}$ (Zhao et al., 2014), with 6.3 μg m$^{-3}$ attributed to hydrocarbon-like IVOCs and 4.2 μg m$^{-3}$ attributed to oxygenated IVOCs. However, this observed estimate of oxygenated IVOCs is conservative (lower bound) based

300 on the experimental method employed by Zhao et al. (2014). Thus, the predicted nonoxygenated IVOC mass, which includes contributions from both mobile and VCP sources, reproduces observations with high fidelity. CMAQ, which only considers IVOCs from VCP and mobile sectors, underpredicts the mass of oxygenated IVOCs by 38%, suggesting additional missing products of oxidation or emissions.

305 The new SOA systems combined with traditional SOA precursors in CMAQ resulted in an effective SOA yield for the VCP sector – defined as the emission-weighted average of the individual species' mass-based SOA yields – of 5.6% for Los Angeles County. This Los Angeles County yield is in good agreement with the work of Qin et al. (2021), that found a 5% yield led to SOA predictions consistent with ambient observational constraints. The U.S. effective VCP SOA yield (5.3%) is only slightly lower than the yield expected for Los Angeles, due to differences stemming from the variability in the

310 composition of VCP emissions nationwide versus in Los Angeles.

## 3.2 CMAQ results

### 3.2.1 SOA

315

Modeled PM$_1$ SOA increased considerably in response to the newly implemented VCP emissions and chemistry, bringing model predictions into closer agreement with observations. Daily maximum PM$_1$ SOA concentrations increased from 1.4 µg m$^{-3}$ (-79% mean bias) in the zero VCP case to 2.8 µg m$^{-3}$ (-58% mean bias) in the CMAQv5.3.2+VCP case, compared to the observed peak value of 6.6 µg m$^{-3}$ (Figure 3a). The diurnal distributions resulted from photochemistry and the sinusoidal

320 distribution of VCP emissions that peak at 12:00 local time. Modeled SOA concentrations improved for all mass loadings and all hours of the day, with the slope of modeled versus observed concentrations increasing from 0.23 in the zero VCP case to 0.43 in the CMAQv5.3.2+VCP case (Figure 4a). Results for the CMAQv5.3.2 case are given in Figs. S3 and S4. Modeled PM$_{2.5}$ SOA displayed similar behavior as PM$_1$ SOA; i.e. the organic fraction and secondary organic fraction of PM$_{2.5}$ was only marginally smaller than the corresponding fractions of PM$_1$ and followed the same diurnal pattern.

325
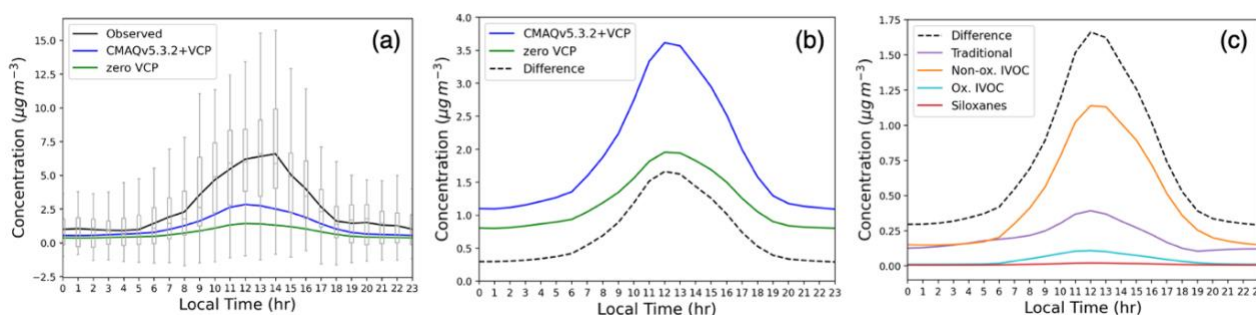
**Figure 3. a) Average hourly concentrations of background-corrected PM$_1$ SOA observed and simulated by the zero VCP and CMAQv5.3.2+VCP modeling cases May 15-June 15. Box and whiskers show all hourly concentrations observed by AMS at the CalNex site. A constant background value was removed from all observed concentrations according to the method in Hayes et al.**
330 **(2015). The background value of each simulation was determined by averaging the lower 50% of hourly concentrations from 00:00 LT to 04:00 LT and subtracting that from each curve. b) Average hourly concentration of total (not size-resolved) SOA for the two simulation cases and their difference (CMAQv5.3.2+VCP – zero VCP). c) Difference in hourly concentrations of total SOA by category.**

The difference between hourly averaged total SOA concentrations in the zero VCP and CMAQv5.3.2+VCP case are shown
335 in Figure 3b and the contributions to that difference from categories of SOA surrogates are shown in Figure 3c. Of the three new categories of VCP emissions, nonoxygenated IVOC precursors formed the most SOA in CMAQ. The increased SOA from the nonoxygenated IVOC VCP precursors reached a peak concentration of 1.14 µg m$^{-3}$, equal to 69% of the total noontime difference. This can be explained by the high SOA yields of the individual species (Fig. S1) and the model surrogates. SOA from oxygenated IVOC VCP precursors reached a peak concentration of 0.11 µg m$^{-3}$ (6.7% of the SOA
340 difference). While oxygenated IVOC emissions were similar in abundance to nonoxygenated IVOC emissions (Figure 2), these species lead to less SOA formation due to their lower SOA yields (Fig. S1). Higher degrees of oxygenation tend to

promote fragmentation upon reaction with OH (Jimenez et al., 2009), producing smaller molecules with higher volatilities and lower potential to form SOA. Siloxanes similarly formed very little SOA, reaching a maximum of 21 ng m$^{-3}$ (1.3% of the SOA difference) at noon. Despite having nonnegligible SOA yields (Fig. S1), siloxanes react with OH on long time

345    scales (Table 1). As such, this results in low localized SOA mass, which is consistent with other modeling and laboratory studies that have predicted siloxanes to form SOA on the order of ng m$^{-3}$ or less (Charan et al., 2021; Milani et al., 2021; Janechek et al., 2017).

Despite traditional species accounting for the greatest fraction of VCP SOA precursor emissions that lead to SOA formation

350    (Figure 2), they contributed only 23% (0.39 μg m$^{-3}$) of the increased noontime SOA in the CMAQv5.3.2+VCP case. These traditional SOA precursors form SOA less efficiently than the IVOC surrogates (Fig. S1), so they result in less SOA formation than IVOCs despite higher emissions.
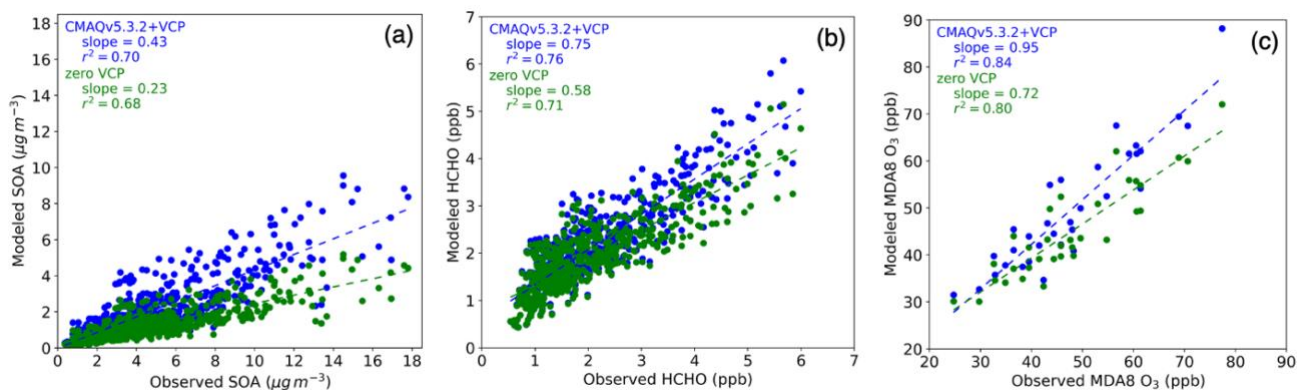
355    **Figure 4. Modeled concentrations predicted by CMAQ zero VCP case (green) and CMAQv5.3.2+VCP case (blue) vs. observations from the CalNex Pasadena ground site. a) Hourly PM$_1$ SOA. b) Hourly formaldehyde (HCHO). c) MDA8 O$_3$. Background values were not removed from any panels.**

The SOA from VCP IVOCs reached a daily maximum of 1.25 μg m$^{-3}$ on average at noon (Figure 3c). IVOCs from mobile sources contributed an additional 1.1 μg m$^{-3}$ at noon (Lu et al., 2020). Therefore this updated CMAQ model predicted a total

360    IVOC-derived SOA concentration of 2.35 μg m$^{-3}$, equivalent to 35% of the total observed above-background PM$_1$ SOA concentration (6.6 μg m$^{-3}$). Previous work stated that 40-85% of above-background SOA concentrations in Pasadena are attributable to S/IVOCs (Hayes et al., 2015), suggesting that additional processes are still needed in the model. This will be discussed further in Section 3.3.

365    **3.2.2 Formaldehyde**

Formaldehyde is one of the most abundant VOCs in the atmosphere and observations of this compound can serve many purposes. Biomass burning, vehicles, and other urban sources emit formaldehyde, and because of its short lifetime (~hours), it can serve as a proxy for local organic emissions. It is also formed in the atmosphere when VOCs undergo radical reactions,

370    oxidize, and fragment, so it serves as an indicator for SOA chemistry since it is formed by many of the same reactions that also lead to SOA formation (Seinfeld & Pandis, 2016). In addition, it is depleted by photolysis and is an important source of radical initiation reactions (Griffith et al., 2016). Formaldehyde can be retrieved directly by satellites (Levelt et al., 2018), which can be used to validate ground data, evaluate model predictions, and predict OA concentrations remotely (Liao et al., 2019). For all of these reasons, formaldehyde is a useful indicator of VOC chemistry in a model.

375

Predicted formaldehyde concentrations improved in response to the new VCP emissions and chemistry, indicating that model updates improve the representation of VOC chemistry beyond SOA in the model. Similar to predicted SOA, formaldehyde concentrations increased at all times, with the ratio of modeled to observed values increasing from 0.58 in the zero VCP case to 0.75 in the CMAQv5.3.2+VCP case (Figure 4b). The diurnal profile of hourly averaged formaldehyde

380    concentrations is given in Fig. S3. The increase in formaldehyde was predominantly due to the increased magnitude of VCP emissions. This work focused primarily on improving the representation of SOA from VCPs, so radical chemistry for the new SOA precursors was treated using existing alkane-like behavior (surrogates ALK1/2/3/4/5). With a more detailed representation of VCP radical chemistry, it is expected that predicted formaldehyde concentrations will improve further.

385    **3.2.3 Ozone**

The bias in predicted ozone concentrations was also reduced by including VCP chemistry. The ratio of modeled to observed concentrations increased from 0.72 in the zero VCP case to 0.95 in the CMAQv5.3.2+VCP case (Figure 4c). Improved ozone is also seen for all operational AQS sites in the California modeling domain, with the modeled to observed ratio

390    increasing from 0.63 in the zero VCP case to 0.70 in the CMAQv5.3.2+VCP case (Fig. S5). The diurnal profile of hourly averaged ozone concentrations is given in Fig. S3. As stated in Section 3.2.2, this study focused on VCP behavior in relation to SOA formation and used existing model species to capture ozone formation. Future work focusing on the ozone chemistry of VCPs could change the magnitude and diurnal profile of predicted ozone.

395    Assuming ozone can serve as a proxy for oxidation rates, the increase in ozone concentration relative to the increase in SOA concentration provides information about the proportional impact of oxidant level versus combined emissions and chemistry on total SOA mass. Average noontime total SOA mass increased from 1.96 $\mu g\ m^{-3}$ in the zero VCP case to 3.62 $\mu g\ m^{-3}$ in the CMAQv5.3.2+VCP case (Figure 3b), an increase of 84.7%. The average noontime ozone concentration increased from 43.0 ppb in the zero VCP case to 49.2 ppb in the CMAQv5.3.2+VCP case (Fig. S3c), an increase of 14.4%. This suggests that the

400    emissions and chemistry updates were approximately 5 times [ (84.7% - 14.4%) / 14.4%] more effective than enhanced

oxidant levels from VCPs in increasing SOA. Additionally, we note that PM$_1$ SOA increased most in the CMAQv5.3.2+VCP case, with little increase in the CMAQv5.3.2 case compared to the zero VCP case (Fig. S3a). In contrast, ozone increased linearly between the three simulation cases (Fig. S3c). The oxidant burden increased noticeably in the CMAQv5.3.2 case but did not equate to a large increase in PM$_1$ SOA, supporting the idea that the oxidant level alone does

405    not have a large influence on enhancing SOA if the relevant precursor pathways are not implemented.

### 3.3 Features of remaining model bias

The residual PM$_1$ SOA bias in Pasadena is well-correlated with ambient temperature (Figure 5a). PM$_1$ SOA bias is defined

410    as modeled hourly concentrations minus observed hourly concentrations. At cooler temperatures in the overnight hours, bias is low and fluctuates around zero. However, as temperature increases towards midday and SOA concentrations increase, the bias becomes more negative, indicating greater model underprediction.

The correlation between SOA bias and temperature is likely caused in part by the inclusion and representation of S/IVOCs

415    emissions and their chemistry in the model. Previous work demonstrated that observed OA in Los Angeles is positively correlated with temperature, and declining OA concentrations have been due largely to reductions of temperature-independent OA. Because this corresponds to a decline in anthropogenic emissions, they suggest that anthropogenically-derived OA is largely temperature-independent while biogenically-derived OA is largely temperature-dependent (Nussbaumer & Cohen, 2021). Our results indicate that OA concentrations are positively correlated with temperature,

420    consistent with the observed Los Angeles OA. The correlation is driven by the larger, secondary portion of OA, rather than POA (Fig. S7). However, the improvement to predicted SOA between simulation cases was seen unequally at different temperatures, as indicated by the larger reduction in absolute model bias at higher temperatures (Figure 5a). This suggests that the SOA derived from VCP species have a temperature-dependent response, in addition to the biogenic emissions cited in Nussbaumer & Cohen (2021). In particular, because nonoxygenated IVOCs were the dominant source of increased SOA

425    predicted by the CMAQv5.3.2+VCP simulation, this work suggests that S/IVOCs are an important source of temperature-dependent SOA in Los Angeles.

Because S/IVOCs have been shown to be a major constituent of modeled SOA and contribute to the correlation between SOA bias and temperature, other sources of S/IVOCs emissions may account for some of the remaining residual SOA bias in

430    the model. For example, asphalt emissions are proposed to contribute 8-30% of total S/IVOC emissions in the South Coast Air Basin in Southern California and have SOA mass yields exceeding 10% (Khare et al., 2020). Their potential to form SOA is very large, and because asphalt emissions are highly temperature-dependent, the SOA increase would be seen largely during midday resulting in an improvement of high-temperature SOA bias. In addition, the underprediction of oxygenated

gas-phase IVOCs (Section 3.1) suggests that additional sources of oxygenated IVOC precursors may be missing from the
435    complete inventory.
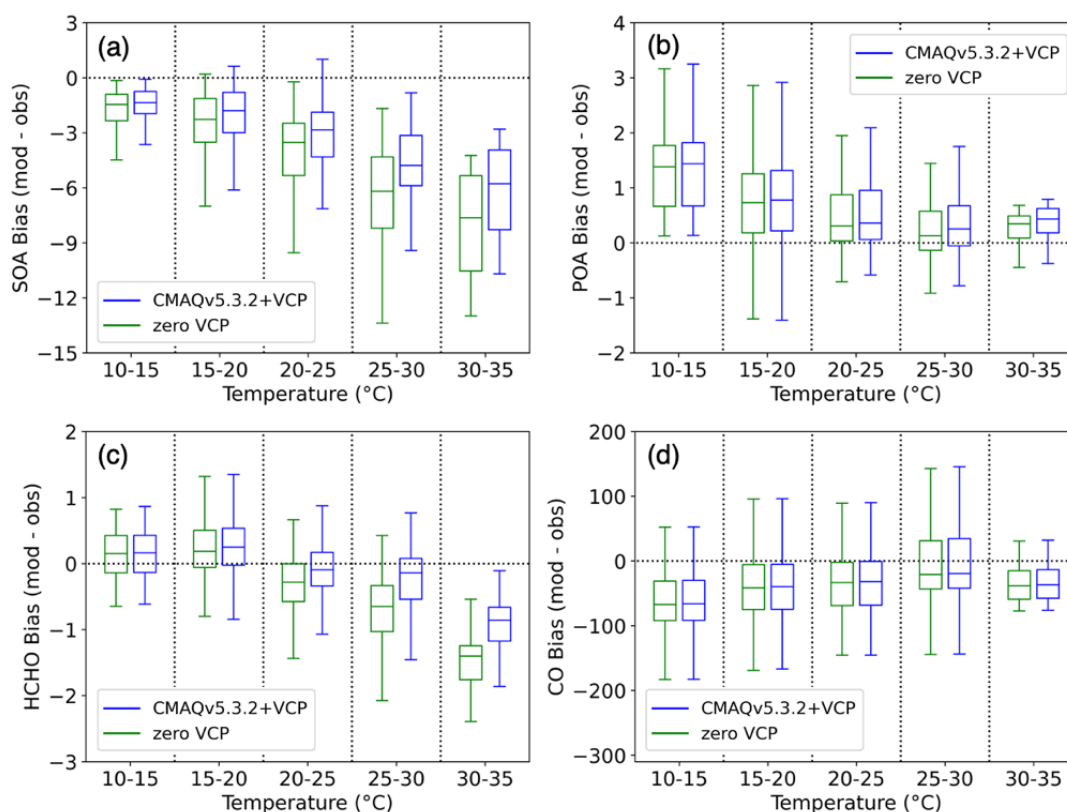
**Figure 5. Bias (modeled - observed) of hourly concentrations vs. modeled temperature for the zero VCP case (green) and
CMAQv5.3.2+VCP case (blue). Hourly concentrations are binned into five temperature ranges of 5°C each and the data in each
440    bin is represented by a box-and-whisker plot. The horizontal midline depicts the median of the data, the edges of the box extend
from the lower to upper quartile of the data, and the whiskers extend from the minimum to the maximum of the data. a) PM$_1$ SOA
bias (µg m$^{-3}$). b) PM$_1$ POA bias (µg m$^{-3}$). c) Formaldehyde (HCHO) bias (ppb). d) CO bias (ppb).**

Formaldehyde, CO, and POA are often used to understand the atmospheric evolution of SOA because they are products of
the same anthropogenic activity and/or VOC oxidation chemistry that forms SOA. As such, they can be used to better
445    understand the remaining sources of error in the model. POA is formed via combustion from vehicles, industrial processes,
cooking, and biomass burning (Jathar et al., 2014; Huffman et al., 2009). CO and formaldehyde are emitted from many
processes and formed as products of atmospheric VOC oxidation (Seinfeld & Pandis, 2016). These species are often used to
understand the effect of dilution on SOA (Hayes et al., 2013). Dilution is caused both by atmospheric transport away from
emission sources, as well as the change in planetary boundary layer (PBL) height over the diurnal cycle. VCPs do not emit
450    POA, CO, or formaldehyde, so any changes observed in their simulated concentrations were caused by chemical and
physical processing in the existing model.

The POA bias did not express the same temperature dependence as SOA. Since VCPs do not emit POA and all other emission sources were consistent between simulation cases, the slight increase in POA concentrations (Figs. 5 and S7) is due to increased partitioning into the particle-phase resulting from higher total OA mass loadings. The POA bias can be exclusively attributed to errors in combustion source emissions inventories and meteorological effects. The combustion source inventories also include emissions of gaseous SOA precursors, which may be incorrectly modeled even if the POA emissions are accurate, especially for cooking and biomass burning sources. While the POA bias does decrease with increasing temperature, it is positive at all temperatures and does not have larger underpredictions at higher temperatures (Figure 5b). Thus POA is not affected in the same way in the model by the processes causing the temperature-dependence of SOA bias. Due to the inconsistency between POA and SOA behavior, errors influencing the emission and transport of POA can likely not be used to describe the temperature dependence of SOA bias. The POA bias also does not provide information about the error in vapor emissions from combustion sources – including S/IVOCs – and their temperature-dependence, and improving combustion emissions inventories may help to close the model-observation gap for SOA.

CO is often used to account for the effects of dilution by scaling SOA to CO enhancement ($\Delta CO = CO - CO_{background}$). Negligible changes in the CO concentration were found between simulation cases considered here (Fig. S3) and the model CO bias is uncorrelated with temperature (Figure 5d). The consistency of predicted CO concentration between cases implies that CO is not affected by the emissions changes to the VCP sector and thus cannot separate SOA formation efficiency from lack of emitted precursors. CO enhancement serves as an effective indicator and correction factor for mobile source emissions in urban areas (e.g. Hayes et al., 2013; Ensberg et al., 2014; Woody et al., 2016), but this work indicates that CO is not an effective tracer for distinguishing VCPs from other sources.

Another potential factor that could influence the temperature-dependence of SOA bias is modeled PBL height. Previous studies that used the same modeled meteorological data as this study (Lu et al., 2020) showed that the modeled PBL height in Pasadena tends to be overestimated during midday and underestimated overnight compared to ceilometer data, which could result in a dilution effect matching the temperature dependence seen in Figure 5a. However, the predicted CO bias does not depend on temperature, which implies that modeled PBL height is not an important driver of the SOA bias temperature-dependence.

In contrast to POA and CO, the formaldehyde bias demonstrated the same trend with temperature as SOA (Figure 5c). This suggests that formaldehyde is affected by emissions, chemistry, and dilution changes similarly to SOA. This is supported by the stronger correlation seen between SOA and formaldehyde compared to the correlation between SOA and POA or CO (Fig. S8). As stated above, the behavior of POA and CO bias suggest that errors in combustion emissions and PBL height cannot fully describe the temperature-dependence of SOA bias, and POA and CO are better indicators of mobile and

industrial sources. Formaldehyde may instead serve as a better indicator of SOA production in urban areas where VCPs are important atmospheric constituents. This may be particularly true for SOA formed from S/IVOCs, which we have shown to be a dominant source of SOA in Los Angeles. Therefore, formaldehyde may provide more information about the errors in modeling SOA formation. The VCP inventory includes near-zero emissions of formaldehyde, but formaldehyde is emitted
490 from wooden furniture and emission rates increase with temperature (Y. Wang et al., 2021). This may account for some of the temperature-dependence of formaldehyde bias, but likely not the entirety since the VCP emissions inventory has been evaluated with select ambient VOC measurements with low error (Seltzer et al., 2021). Because formaldehyde is a major product of VOC oxidation, the temperature-dependence of both SOA and formaldehyde may suggest that additional missing chemistry may be causing some of the error. Chemical processes that have not been included in the mechanism include
495 autooxidation (Crounse et al., 2013), detailed chemistry of oxygenated precursors, and formaldehyde potentially formed from the fragmentation of S/IVOC precursors to SOA. Future work must investigate the importance of these factors and tracking the response of formaldehyde to these changes could provide insight. As mobile-source emissions decline and VCP emissions become the dominant source of aerosol in urban areas, formaldehyde should be considered an important indicator for SOA production from VCPs.

500

**4 Conclusions and future work**

We have shown that VCPs are a major source of SOA in urban atmospheres by introducing updated emissions and VCP-relevant chemistry into CMAQ that better represents SOA precursors emitted from these sources. This includes three new
505 categories of emissions: siloxanes, oxygenated IVOCs, and nonoxygenated IVOCs. VCP emissions from the VCPy framework (Seltzer et al., 2021) were used to parameterize the new chemistry, and the mapping of VCP emitted species to model surrogates was reviewed and updated based on species structure, volatility, and estimated SOA yield.

The new model chemistry and emissions inventory doubles the predicted SOA concentrations above background levels,
510 increasing the average daily maximum $PM_1$ SOA concentration by 1.4 $\mu$g m$^{-3}$, equating to a 21% decrease in the absolute mean bias. Most of the increased SOA mass was formed from nonoxygenated IVOC VCP precursors, followed by SOA formed from traditional VOC precursors and oxygenated IVOC precursors, with little SOA formed from siloxanes. Improvements were additionally seen in simulated formaldehyde and ozone concentrations.

515 Future work should consider how VCP emissions have evolved over time. VCPy version 1.0 requires information about VCP product composition and usage patterns from broad sources, including product surveys, economic statistics, and population distributions. These metrics change over time and will affect both the speciation and emission rates of organic compounds from VCPs. Diurnal and seasonal patterns of VCP emissions should also be updated to reflect more recent observations (Gkatzelis et al., 2021).

520

The remaining error in VCP-derived SOA predictions may reflect our lack of understanding about the oxidation pathways of low-volatility and/or oxygenated species. More information is needed about the structure, volatility, and reactivity of the products of atmospheric oxidation reactions, plus the impacts of wall loss and $NO_x$ concentrations on SOA yields from experiments, so that models and parameterizations like the VBS can be developed. As this data become available, models can be improved to represent SOA formation from oxygenated precursors and S/IVOCs emitted from VCPs. In addition, the correlation between SOA concentration bias and temperature suggests residual model error is associated with missing sources of S/IVOC emissions, including emissions from asphalt (Khare et al., 2020), combustion sources, and other S/IVOCs that have large potential to form SOA. The formaldehyde bias demonstrates a similar relationship to temperature as SOA bias, implying that formaldehyde can serve as a representative tracer of VOC chemistry to investigate the formation of SOA from VCPs. Including S/IVOC emissions and their atmospheric chemistry will be important for future air quality models.

**Data Availability**

CalNex observations are publicly available at https://csl.noaa.gov/groups/csl7/measurements/2010calnex/. The full VCPy dataset is available by downloading VCPyv1.0 at https://doi.org/10.23719/1520157. The SAPRC07TIC_AE7I_VCP speciation profile, CMAQ chemical mechanism source code, and CMAQ output will be posted on data.gov upon final publication.

**Supplement**

The supplement related to this article is available online at: ___

**Author Contributions**

HOTP, KMS, and EAP designed the research. EAP and KMS implemented the mechanism in CMAQv5.3.2 and ran the simulations. All authors participated in data analysis and discussions. EAP drafted the paper with input from all coauthors.

545

**Acknowledgements**

The authors thank Christopher Cappa, Wyat Appel, and Ben Schulze for modeling support and helpful discussions.

**Financial Support**

Karl Seltzer and Elyse Pennington were supported by the Oak Ridge Institute for Science and Education (ORISE) Research Participation Program for the U.S. Environmental Protection Agency (EPA). Elyse Pennington was also supported by a Global Research Outreach (GRO) award from the Samsung Advanced Institute of Technology (SAIT).

**Competing Interests**

555     The authors declare that they have no competing interests.

**Disclaimer**

Although this work was contributed by research staff in the Environmental Protection Agency and has been reviewed and
approved for publication, it does not reflect official policy of the

560     EPA. The views expressed in this document are solely those of authors and do not necessarily reflect those of the Agency.
EPA does not endorse any products or commercial services mentioned in this publication.

**References**

565     AE7I Species Table. (2021). U.S. Environmental Protection Agency.
https://github.com/USEPA/CMAQ/blob/72ec4e5681e1ed0b4917792a9a240b0302a303a7/CCTM/src/MECHS/mec
hanism_information/saprc07tic_ae7i_aq/AE7I_species_table.md (Original work published 2016)

Appel, K. W., Bash, J. O., Fahey, K. M., Foley, K. M., Gilliam, R. C., Hogrefe, C., Hutzell, W. T., Kang, D., Mathur, R.,
Murphy, B. N., Napelenok, S. L., Nolte, C. G., Pleim, J. E., Pouliot, G. A., Pye, H. O. T., Ran, L., Roselle, S. J.,
570     Sarwar, G., Schwede, D. B., … Wong, D. C. (2021). The Community Multiscale Air Quality (CMAQ) model
versions 5.3 and 5.3.1: System updates and evaluation. Geoscientific Model Development, 14(5), 2867–2897.
https://doi.org/10.5194/gmd-14-2867-2021

Baker, K. R., Carlton, A. G., Kleindienst, T. E., Offenberg, J. H., Beaver, M. R., Gentner, D. R., Goldstein, A. H., Hayes, P.
L., Jimenez, J. L., Gilman, J. B., Gouw, J. A. de, Woody, M. C., Pye, H. O. T., Kelly, J. T., Lewandowski, M.,
575     Jaoui, M., Stevens, P. S., Brune, W. H., Lin, Y.-H., … Surratt, J. D. (2015). Gas and aerosol carbon in California:
Comparison of measurements and model predictions in Pasadena and Bakersfield. Atmospheric Chemistry and
Physics, 15(9), 5243–5258. https://doi.org/10.5194/acp-15-5243-2015

Bash, J. O., Baker, K. R., & Beaver, M. R. (2016). Evaluation of improved land use and canopy representation in BEIS
v3.61 with biogenic VOC measurements in California. Geoscientific Model Development, 9(6), 2191–2207.
580     https://doi.org/10.5194/gmd-9-2191-2016

Binkowski, F. S., & Roselle, S. J. (2003). Models-3 Community Multiscale Air Quality (CMAQ) model aerosol component
1. Model description. Journal of Geophysical Research: Atmospheres, 108(D6).
https://doi.org/10.1029/2001JD001409

Cappa, C. D., & Wilson, K. R. (2012). Multi-generation gas-phase oxidation, equilibrium partitioning, and the formation and
585     evolution of secondary organic aerosol. Atmospheric Chemistry and Physics, 12(20), 9505–9528.
https://doi.org/10.5194/acp-12-9505-2012

Carter, W. P. L. (2010). Development of the SAPRC-07 chemical mechanism. Atmospheric Environment, 44(40), 5324–5335. https://doi.org/10.1016/j.atmosenv.2010.01.026

Charan, S. M., Buenconsejo, R. S., & Seinfeld, J. H. (2020). Secondary organic aerosol yields from the oxidation of benzyl alcohol. Atmospheric Chemistry and Physics, 20(21), 13167–13190. https://doi.org/10.5194/acp-20-13167-2020

Charan, S. M., Huang, Y., Buenconsejo, R. S., Li, Q., Cocker III, D. R., & Seinfeld, J. H. (2021). Secondary Organic Aerosol Formation from the Oxidation of Decamethylcyclopentasiloxane at Atmospherically Relevant OH Concentrations. Atmospheric Chemistry and Physics Discussions, 1–17. https://doi.org/10.5194/acp-2021-353

Coggon, M. M., McDonald, B. C., Vlasenko, A., Veres, P. R., Bernard, F., Koss, A. R., Yuan, B., Gilman, J. B., Peischl, J., Aikin, K. C., DuRant, J., Warneke, C., Li, S.-M., & de Gouw, J. A. (2018). Diurnal Variability and Emission Pattern of Decamethylcyclopentasiloxane (D5) from the Application of Personal Care Products in Two North American Cities. Environmental Science & Technology, 52(10), 5610–5618. https://doi.org/10.1021/acs.est.8b00506

Crounse, J. D., Nielsen, L. B., Jørgensen, S., Kjaergaard, H. G., & Wennberg, P. O. (2013). Autoxidation of Organic Compounds in the Atmosphere. The Journal of Physical Chemistry Letters, 4(20), 3513–3520. https://doi.org/10.1021/jz4019207

Donahue, N. M., Epstein, S. A., Pandis, S. N., & Robinson, A. L. (2011). A two-dimensional volatility basis set: 1. organic-aerosol mixing thermodynamics. Atmospheric Chemistry and Physics, 11(7), 3303–3318. https://doi.org/10.5194/acp-11-3303-2011

Ensberg, J. J., Hayes, P. L., Jimenez, J. L., Gilman, J. B., Kuster, W. C., de Gouw, J. A., Holloway, J. S., Gordon, T. D., Jathar, S., Robinson, A. L., & Seinfeld, J. H. (2014). Emission factor ratios, SOA mass yields, and the impact of vehicular emissions on SOA formation. Atmospheric Chemistry and Physics, 14(5), 2383–2397. https://doi.org/10.5194/acp-14-2383-2014

Epstein, S. A., Riipinen, I., & Donahue, N. M. (2010). A Semiempirical Correlation between Enthalpy of Vaporization and Saturation Concentration for Organic Aerosol. Environmental Science & Technology, 44(2), 743–748. https://doi.org/10.1021/es902497z

Gkatzelis, G. I., Coggon, M. M., McDonald, B. C., Peischl, J., Aikin, K. C., Gilman, J. B., Trainer, M., & Warneke, C. (2021). Identifying Volatile Chemical Product Tracer Compounds in U.S. Cities. Environmental Science & Technology, 55(1), 188–199. https://doi.org/10.1021/acs.est.0c05467

Goldstein, A. H., & Galbally, I. E. (2007). Known and Unexplored Organic Constituents in the Earth's Atmosphere. Environmental Science & Technology, 41(5), 1514–1521. https://doi.org/10.1021/es072476p

Griffith, S. M., Hansen, R. F., Dusanter, S., Michoud, V., Gilman, J. B., Kuster, W. C., Veres, P. R., Graus, M., Gouw, J. A. de, Roberts, J., Young, C., Washenfelder, R., Brown, S. S., Thalman, R., Waxman, E., Volkamer, R., Tsai, C., Stutz, J., Flynn, J. H., … Stevens, P. S. (2016). Measurements of hydroxyl and hydroperoxy radicals during

620      CalNex-LA: Model comparisons and radical budgets. Journal of Geophysical Research: Atmospheres, 121(8), 4211–4232. https://doi.org/10.1002/2015JD024358

Hayes, P. L., Carlton, A. G., Baker, K. R., Ahmadov, R., Washenfelder, R. A., Alvarez, S., Rappenglück, B., Gilman, J. B., Kuster, W. C., de Gouw, J. A., Zotter, P., Prévôt, A. S. H., Szidat, S., Kleindienst, T. E., Offenberg, J. H., Ma, P. K., & Jimenez, J. L. (2015). Modeling the formation and aging of secondary organic aerosols in Los Angeles during
625      CalNex 2010. Atmospheric Chemistry and Physics, 15(10), 5773–5801. https://doi.org/10.5194/acp-15-5773-2015

Hayes, P. L., Ortega, A. M., Cubison, M. J., Froyd, K. D., Zhao, Y., Cliff, S. S., Hu, W. W., Toohey, D. W., Flynn, J. H., Lefer, B. L., Grossberg, N., Alvarez, S., Rappenglück, B., Taylor, J. W., Allan, J. D., Holloway, J. S., Gilman, J. B., Kuster, W. C., Gouw, J. A. de, … Jimenez, J. L. (2013). Organic aerosol composition and sources in Pasadena, California, during the 2010 CalNex campaign. Journal of Geophysical Research: Atmospheres, 118(16), 9233–
630      9257. https://doi.org/10.1002/jgrd.50530

Hodzic, A., Aumont, B., Knote, C., Lee-Taylor, J., Madronich, S., & Tyndall, G. (2014). Volatility dependence of Henry's law constants of condensable organics: Application to estimate depositional loss of secondary organic aerosols. Geophysical Research Letters, 41(13), 4795–4804. https://doi.org/10.1002/2014GL060649

Huffman, J. A., Docherty, K. S., Mohr, C., Cubison, M. J., Ulbrich, I. M., Ziemann, P. J., Onasch, T. B., & Jimenez, J. L.
635      (2009). Chemically-Resolved Volatility Measurements of Organic Aerosol from Different Sources. Environmental Science & Technology, 43(14), 5351–5357. https://doi.org/10.1021/es803539d

Hyslop, N. P. (2009). Impaired visibility: The air pollution people see. Atmospheric Environment, 43(1), 182–195. https://doi.org/10.1016/j.atmosenv.2008.09.067

Intergovernmental Panel on Climate Change (Ed.). (2014). Anthropogenic and Natural Radiative Forcing. In Climate
640      Change 2013 – The Physical Science Basis: Working Group I Contribution to the Fifth Assessment Report of the Intergovernmental Panel on Climate Change (pp. 659–740). Cambridge University Press. https://doi.org/10.1017/CBO9781107415324.018

Janechek, N. J., Hansen, K. M., & Stanier, C. O. (2017). Comprehensive atmospheric modeling of reactive cyclic siloxanes and their oxidation products. Atmospheric Chemistry and Physics, 17(13), 8357–8370. https://doi.org/10.5194/acp-
645      17-8357-2017

Janechek, N. J., Marek, R. F., Bryngelson, N., Singh, A., Bullard, R. L., Brune, W. H., & Stanier, C. O. (2019). Physical properties of secondary photochemical aerosol from OH oxidation of a cyclic siloxane. Atmospheric Chemistry and Physics, 19(3), 1649–1664. https://doi.org/10.5194/acp-19-1649-2019

Jathar, S. H., Gordon, T. D., Hennigan, C. J., Pye, H. O. T., Pouliot, G., Adams, P. J., Donahue, N. M., & Robinson, A. L.
650      (2014). Unspeciated organic emissions from combustion sources and their influence on the secondary organic aerosol budget in the United States. Proceedings of the National Academy of Sciences, 111(29), 10473–10478. https://doi.org/10.1073/pnas.1323740111

Jathar, S. H., Woody, M., Pye, H. O. T., Baker, K. R., & Robinson, A. L. (2017). Chemical transport model simulations of organic aerosol in southern California: Model evaluation and gasoline and diesel source contributions. Atmospheric Chemistry and Physics, 17(6), 4305–4318. https://doi.org/10.5194/acp-17-4305-2017

Jimenez, J. L., Canagaratna, M. R., Donahue, N. M., Prevot, A. S. H., Zhang, Q., Kroll, J. H., DeCarlo, P. F., Allan, J. D., Coe, H., Ng, N. L., Aiken, A. C., Docherty, K. S., Ulbrich, I. M., Grieshop, A. P., Robinson, A. L., Duplissy, J., Smith, J. D., Wilson, K. R., Lanz, V. A., … Worsnop, D. R. (2009). Evolution of Organic Aerosols in the Atmosphere. Science, 326(5959), 1525–1529. https://doi.org/10.1126/science.1180353

Khare, P., & Gentner, D. R. (2018). Considering the future of anthropogenic gas-phase organic compound emissions and the increasing influence of non-combustion sources on urban air quality. Atmospheric Chemistry and Physics, 18(8), 5391–5413. https://doi.org/10.5194/acp-18-5391-2018

Khare, P., Machesky, J., Soto, R., He, M., Presto, A. A., & Gentner, D. R. (2020). Asphalt-related emissions are a major missing nontraditional source of secondary organic aerosol precursors. Science Advances, 6(36), eabb9785. https://doi.org/10.1126/sciadv.abb9785

Levelt, P. F., Joiner, J., Tamminen, J., Veefkind, J. P., Bhartia, P. K., Stein Zweers, D. C., Duncan, B. N., Streets, D. G., Eskes, H., van der A, R., McLinden, C., Fioletov, V., Carn, S., de Laat, J., DeLand, M., Marchenko, S., McPeters, R., Ziemke, J., Fu, D., … Wargan, K. (2018). The Ozone Monitoring Instrument: Overview of 14 years in space. Atmospheric Chemistry and Physics, 18(8), 5699–5745. https://doi.org/10.5194/acp-18-5699-2018

Li, L., & Cocker, D. R. (2018). Molecular structure impacts on secondary organic aerosol formation from glycol ethers. Atmospheric Environment, 180, 206–215. https://doi.org/10.1016/j.atmosenv.2017.12.025

Li, W., Li, L., Chen, C., Kacarab, M., Peng, W., Price, D., Xu, J., & Cocker, D. R. (2018). Potential of select intermediate-volatility organic compounds and consumer products for secondary organic aerosol and ozone formation under relevant urban conditions. Atmospheric Environment, 178, 109–117. https://doi.org/10.1016/j.atmosenv.2017.12.019

Li, Y., Rodier, C., Lea, J. D., Harvey, J., & Kleeman, M. J. (2021). Improving spatial surrogates for area source emissions inventories in California. Atmospheric Environment, 247, 117665. https://doi.org/10.1016/j.atmosenv.2020.117665

Liao, J., Hanisco, T. F., Wolfe, G. M., St. Clair, J., Jimenez, J. L., Campuzano-Jost, P., Nault, B. A., Fried, A., Marais, E. A., Gonzalez Abad, G., Chance, K., Jethva, H. T., Ryerson, T. B., Warneke, C., & Wisthaler, A. (2019). Towards a satellite formaldehyde – in situ hybrid estimate for organic aerosol abundance. Atmospheric Chemistry and Physics, 19(5), 2765–2785. https://doi.org/10.5194/acp-19-2765-2019

Lim, S. S., Vos, T., Flaxman, A. D., Danaei, G., Shibuya, K., Adair-Rohani, H., AlMazroa, M. A., Amann, M., Anderson, H. R., Andrews, K. G., Aryee, M., Atkinson, C., Bacchus, L. J., Bahalim, A. N., Balakrishnan, K., Balmes, J., Barker-Collo, S., Baxter, A., Bell, M. L., … Ezzati, M. (2012). A comparative risk assessment of burden of disease and injury attributable to 67 risk factors and risk factor clusters in 21 regions, 1990–2010: A systematic analysis for the

Global Burden of Disease Study 2010. The Lancet, 380(9859), 2224–2260. https://doi.org/10.1016/S0140-6736(12)61766-8

Lu, Q., Murphy, B. N., Qin, M., Adams, P. J., Zhao, Y., Pye, H. O. T., Efstathiou, C., Allen, C., & Robinson, A. L. (2020). Simulation of organic aerosol formation during the CalNex study: Updated mobile emissions and secondary organic aerosol parameterization for intermediate-volatility organic compounds. Atmospheric Chemistry and Physics, 20(7), 4313–4332. https://doi.org/10.5194/acp-20-4313-2020

McDonald, B. C., Gouw, J. A. de, Gilman, J. B., Jathar, S. H., Akherati, A., Cappa, C. D., Jimenez, J. L., Lee-Taylor, J., Hayes, P. L., McKeen, S. A., Cui, Y. Y., Kim, S.-W., Gentner, D. R., Isaacman-VanWertz, G., Goldstein, A. H., Harley, R. A., Frost, G. J., Roberts, J. M., Ryerson, T. B., & Trainer, M. (2018). Volatile chemical products emerging as largest petrochemical source of urban organic emissions. Science, 359(6377), 760–764. https://doi.org/10.1126/science.aaq0524

Milani, A., Al-Naiema, I. M., & Stone, E. A. (2021). Detection of a secondary organic aerosol tracer derived from personal care products. Atmospheric Environment, 246, 118078. https://doi.org/10.1016/j.atmosenv.2020.118078

Murphy, B. N., Nolte, C. G., Sidi, F., Bash, J. O., Appel, K. W., Jang, C., Kang, D., Kelly, J., Mathur, R., Napelenok, S., Pouliot, G., & Pye, H. O. T. (2021). The Detailed Emissions Scaling, Isolation, and Diagnostic (DESID) module in the Community Multiscale Air Quality (CMAQ) modeling system version 5.3.2. Geoscientific Model Development, 14(6), 3407–3420. https://doi.org/10.5194/gmd-14-3407-2021

Murphy, B. N., Woody, M. C., Jimenez, J. L., Carlton, A. M. G., Hayes, P. L., Liu, S., Ng, N. L., Russell, L. M., Setyan, A., Xu, L., Young, J., Zaveri, R. A., Zhang, Q., & Pye, H. O. T. (2017). Semivolatile POA and parameterized total combustion SOA in CMAQv5.2: Impacts on source strength and partitioning. Atmospheric Chemistry and Physics, 17(18), 11107–11133. https://doi.org/10.5194/acp-17-11107-2017

Nussbaumer, C. M., & Cohen, R. C. (2021). Impact of OA on the Temperature Dependence of PM 2.5 in the Los Angeles Basin. Environmental Science & Technology, 55(6), 3549–3558. https://doi.org/10.1021/acs.est.0c07144

Pye, H. O. T., Murphy, B. N., Xu, L., Ng, N. L., Carlton, A. G., Guo, H., Weber, R., Vasilakos, P., Appel, K. W., Budisulistiorini, S. H., Surratt, J. D., Nenes, A., Hu, W., Jimenez, J. L., Isaacman-VanWertz, G., Misztal, P. K., & Goldstein, A. H. (2017). On the implications of aerosol liquid water and phase separation for organic aerosol mass. Atmospheric Chemistry and Physics, 17(1), 343–369. https://doi.org/10.5194/acp-17-343-2017

Pye, H. O. T., Pinder, R. W., Piletic, I. R., Xie, Y., Capps, S. L., Lin, Y.-H., Surratt, J. D., Zhang, Z., Gold, A., Luecken, D. J., Hutzell, W. T., Jaoui, M., Offenberg, J. H., Kleindienst, T. E., Lewandowski, M., & Edney, E. O. (2013). Epoxide Pathways Improve Model Predictions of Isoprene Markers and Reveal Key Role of Acidity in Aerosol Formation. Environmental Science & Technology, 47(19), 11056–11064. https://doi.org/10.1021/es402106h

Qin, M., Murphy, B. N., Isaacs, K. K., McDonald, B. C., Lu, Q., McKeen, S. A., Koval, L., Robinson, A. L., Efstathiou, C., Allen, C., & Pye, H. O. T. (2021). Criteria pollutant impacts of volatile chemical products informed by near-field modelling. Nature Sustainability, 4(2), 129–137. https://doi.org/10.1038/s41893-020-00614-1

720    Robinson, A. L., Donahue, N. M., Shrivastava, M. K., Weitkamp, E. A., Sage, A. M., Grieshop, A. P., Lane, T. E., Pierce, J.
R., & Pandis, S. N. (2007). Rethinking Organic Aerosols: Semivolatile Emissions and Photochemical Aging.
Science, 315(5816), 1259–1262. https://doi.org/10.1126/science.1133061

Ryerson, T. B., Andrews, A. E., Angevine, W. M., Bates, T. S., Brock, C. A., Cairns, B., Cohen, R. C., Cooper, O. R.,
Gouw, J. A. de, Fehsenfeld, F. C., Ferrare, R. A., Fischer, M. L., Flagan, R. C., Goldstein, A. H., Hair, J. W.,

725    Hardesty, R. M., Hostetler, C. A., Jimenez, J. L., Langford, A. O., … Wofsy, S. C. (2013). The 2010 California
Research at the Nexus of Air Quality and Climate Change (CalNex) field study. Journal of Geophysical Research:
Atmospheres, 118(11), 5830–5866. https://doi.org/10.1002/jgrd.50331

Santoni, G. W., Daube, B. C., Kort, E. A., Jiménez, R., Park, S., Pittman, J. V., Gottlieb, E., Xiang, B., Zahniser, M. S.,
Nelson, D. D., McManus, J. B., Peischl, J., Ryerson, T. B., Holloway, J. S., Andrews, A. E., Sweeney, C., Hall, B.,

730    Hintsa, E. J., Moore, F. L., … Wofsy, S. C. (2014). Evaluation of the airborne quantum cascade laser spectrometer
(QCLS) measurements of the carbon and greenhouse gas suite – $CO_2$, $CH_4$, $N_2O$, and CO – during
the CalNex and HIPPO campaigns. Atmospheric Measurement Techniques, 7(6), 1509–1526.
https://doi.org/10.5194/amt-7-1509-2014

Seinfeld, J. H., & Pandis, S. N. (2016). Atmospheric Chemistry and Physics: From Air Pollution to Climate Change (3rd

735    ed.). John Wiley & Sons, Inc.

Seltzer, K. M., Pennington, E., Rao, V., Murphy, B. N., Strum, M., Isaacs, K. K., & Pye, H. O. T. (2021). Reactive organic
carbon emissions from volatile chemical products. Atmospheric Chemistry and Physics, 21(6), 5079–5100.
https://doi.org/10.5194/acp-21-5079-2021

Shah, R. U., Coggon, M. M., Gkatzelis, G. I., McDonald, B. C., Tasoglou, A., Huber, H., Gilman, J., Warneke, C.,

740    Robinson, A. L., & Presto, A. A. (2020). Urban Oxidation Flow Reactor Measurements Reveal Significant
Secondary Organic Aerosol Contributions from Volatile Emissions of Emerging Importance. Environmental
Science & Technology, 54(2), 714–725. https://doi.org/10.1021/acs.est.9b06531

Shah, T., Shi, Y., Beardsley, R., & Yarwood, G. (2020). Speciation Tool User's Guide Version 5.0. Ramboll US
Corporation.

745    Skamarock, W. C., Klemp, J. B., Dudhia, J., Gill, D. O., & Barker, D. (2008). A Description of the Advanced Research
WRF Version 3 (NCAR/TN-475+STR). University Corporation for Atmospheric Research.
http://dx.doi.org/10.5065/D68S4MVH

US EPA, O. (2013, August 1). Air Quality System (AQS) [Data and Tools]. US EPA. https://www.epa.gov/aqs

US EPA, O. (2015, June 2). National Emissions Inventory (NEI) [Other Policies and Guidance]. US EPA.

750    https://www.epa.gov/air-emissions-inventories/national-emissions-inventory-nei

US EPA Office of Research and Development. (2020). CMAQ. Zenodo. https://doi.org/10.5281/zenodo.4081737

Wang, D.-G., Norwood, W., Alaee, M., Byer, J. D., & Brimble, S. (2013). Review of recent advances in research on the toxicity, detection, occurrence and fate of cyclic volatile methyl siloxanes in the environment. Chemosphere, 93(5), 711–725. https://doi.org/10.1016/j.chemosphere.2012.10.041

Wang, Y., Wang, H., Tan, Y., Liu, J., Wang, K., Ji, W., Sun, L., Yu, X., Zhao, J., Xu, B., & Xiong, J. (2021). Measurement of the key parameters of VOC emissions from wooden furniture, and the impact of temperature. Atmospheric Environment, 118510. https://doi.org/10.1016/j.atmosenv.2021.118510

Warneke, C., Veres, P., Holloway, J. S., Stutz, J., Tsai, C., Alvarez, S., Rappenglueck, B., Fehsenfeld, F. C., Graus, M., Gilman, J. B., & de Gouw, J. A. (2011). Airborne formaldehyde measurements using PTR-MS: Calibration, humidity dependence, inter-comparison and initial results. Atmospheric Measurement Techniques, 4(10), 2345–2358. https://doi.org/10.5194/amt-4-2345-2011

Woody, M. C., Baker, K. R., Hayes, P. L., Jimenez, J. L., Koo, B., & Pye, H. O. T. (2016). Understanding sources of organic aerosol during CalNex-2010 using the CMAQ-VBS. Atmospheric Chemistry and Physics, 16(6), 4081–4100. https://doi.org/10.5194/acp-16-4081-2016

Wu, Y., & Johnston, M. V. (2017). Aerosol Formation from OH Oxidation of the Volatile Cyclic Methyl Siloxane (cVMS) Decamethylcyclopentasiloxane. Environmental Science & Technology, 51(8), 4445–4451. https://doi.org/10.1021/acs.est.7b00655

Xie, Y., Paulot, F., Carter, W. P. L., Nolte, C. G., Luecken, D. J., Hutzell, W. T., Wennberg, P. O., Cohen, R. C., & Pinder, R. W. (2013). Understanding the impact of recent advances in isoprene photooxidation on simulations of regional air quality. Atmospheric Chemistry and Physics, 13(16), 8439–8455. https://doi.org/10.5194/acp-13-8439-2013

Zhang, Q., Jimenez, J. L., Canagaratna, M. R., Allan, J. D., Coe, H., Ulbrich, I., Alfarra, M. R., Takami, A., Middlebrook, A. M., Sun, Y. L., Dzepina, K., Dunlea, E., Docherty, K., DeCarlo, P. F., Salcedo, D., Onasch, T., Jayne, J. T., Miyoshi, T., Shimono, A., … Worsnop, D. R. (2007). Ubiquity and dominance of oxygenated species in organic aerosols in anthropogenically-influenced Northern Hemisphere midlatitudes. Geophysical Research Letters, 34(13). https://doi.org/10.1029/2007GL029979

Zhao, Y., Hennigan, C. J., May, A. A., Tkacik, D. S., de Gouw, J. A., Gilman, J. B., Kuster, W. C., Borbon, A., & Robinson, A. L. (2014). Intermediate-Volatility Organic Compounds: A Large Source of Secondary Organic Aerosol. Environmental Science & Technology, 48(23), 13743–13750. https://doi.org/10.1021/es5035188

Zhao, Y., Nguyen, N. T., Presto, A. A., Hennigan, C. J., May, A. A., & Robinson, A. L. (2015). Intermediate Volatility Organic Compound Emissions from On-Road Diesel Vehicles: Chemical Composition, Emission Factors, and Estimated Secondary Organic Aerosol Production. Environmental Science & Technology, 49(19), 11516–11526. https://doi.org/10.1021/acs.est.5b02841